Chapter 30
Wave Patterns in a Hippocampal Network

Diogo L. M. Souza, Lucas E. Bentivoglio, Fernando S. Borges, Gustavo A. Sousa, Patrício D. C. dos Reis, Iberê L. Caldas, Ricardo L. Viana, Antonio M. Batista, and Kelly C. Iarosz

Abstract The brain exhibits complex high-order cognitive activity, for instance, traveling waves. In the hippocampus, spatial processing and long-term memory are mediated by such waves. Due to its potential to replicate and explore these oscillatory patterns, mathematical modeling has gained significant attention. In this work, we simulate a hippocampal network and investigate the oscillations that arise within the system. Each neuron is described by the adaptive exponential integrate-and-fire model, interconnected via chemical excitatory synapses. Our findings reveal that

These authors contributed equally to this work.

D. L. M. Souza (✉) · L. E. Bentivoglio · F. S. Borges · P. D. C. dos Reis · A. M. Batista · K. C. Iarosz
Graduate Program in Science, State University of Ponta Grossa, Ponta Grossa, PR, Brazil
e-mail: diogoleonaisouza@gmail.com

F. S. Borges
Department of Physiology and Pharmacology, State University of New York Downstate Health Sciences University, Brooklyn, NY, USA

Center for Mathematics, Computation, and Cognition, Federal University of ABC, SP, Brazil

G. A. Sousa
Undergraduate student of Physics Department, State University of Ponta Grossa, Ponta Grossa, PR, Brazil

I. L. Caldas
Physics Institute, University of São Paulo, SP, Brazil, SP, Brazil

R. L. Viana
Department of Physics, Federal University of Paraná, Curitiba, PR, Brazil

A. M. Batista
Department of Mathematics and Statistics, State University of Ponta Grossa, Ponta Grossa, PR, Brazil

K. C. Iarosz
University Center UNIFATEB, Telêmaco Borba, PR, Brazil

© The Author(s), under exclusive license to Springer Nature Switzerland AG 2025

J. M. Balthazar et al. (eds.), *Nonlinear Dynamics, Chaos, Control, Energy Transfer and Their Applications in Engineering Sciences*, Mechanisms and Machine Science 142, https://doi.org/10.1007/978-3-031-84449-2_30

different combinations of coupling strength and radius of connection produce different wave shapes. Moreover, we demonstrate a method for spiral waves detection. We show that the appearance of multiple spiral waves leads to global desynchronization.

Keywords Brain waves · Hippocampus · Neuronal network

30.1 Introduction

Traveling waves are spatial-temporal patterns that propagate in a medium preserving its velocity and shape [1, 2]. The first observation of traveling waves in the brain was made at the end of the 19th century using electroencephalography (EEG) [3]. In the brain, waves propagate throughout the cortex and hippocampus regions. The coordinated activity of neuronal firing generates waves such as plane, radial and spiral. The combination of these patterns generates complex activities in the neuronal network [4]. The presence of these patterns can be seen in computational simulations and experimental data [5]. For example, a spiral wave pattern has been identified in the neocortex during sleep-like states and pharmacologically induced states. It is theorized that such spatial patterns play a crucial role in organizing and modulating healthy and pathological brain activities, for instance, epilepsy [6].

Communication between brain regions is proposed to be mediated by traveling waves [7]. Wave properties have been shown to be task-driven. Patten et al. [7] have demonstrated that the propagation direction of waves in the cortex is correlated with the reaction speed. In the hippocampus, traveling waves play a vital role in information encoding and communication between the neocortex and hippocampus [8, 9]. Computational experiments have been concluded to deepen our knowledge about hippocampus waves, given their importance in memory and information transmission to the cortex. Molter et al. [10] developed a hippocampus model incorporating synaptic plasticity and theta phase precession which reproduces the patterns of reactivation of places cells in sharp waves. Yao et al. [11] reported that when bounded noise is considered, the intensity and amplitude of the noise influence spiral wave appearance. The appearance of traveling waves is related to information transmission delay and with the topology of the network [12].

In this work, we construct a CA1 hippocampal network composed of pyramidal neurons [13], identified as excitatory. This type of neuronal cell is in a great number in the hippocampus and cortex and they play important roles in cognitive process [14]. We consider point neurons where the electrical activity of each neuron is described by the adaptive exponential integrate-and-fire model (AEIF) [15]. This model consists of two differential equations, one equation describes the membrane potential and the other represents the adaptive current. AEIF model has been extensively applied in epilepsy research [16–18] and to explore complex cognitive tasks in the cortex [19]. We investigate the emergence of distinct wave patterns and synchronization in the network for different radius connections and coupling strengths. Our findings show that different waves emerge in the network and that multiple wave patterns can

coexist. When spiral waves arise a phase singularity is generated in its core, composed of asynchronous neurons. As more spiral waves appear, the global synchronization diminishes. Moreover, we show that the phase singularity of spiral waves produces reduced local synchronization in its location.

30.2 Neuronal Model and Diagnostic Tools

The electrical activity of each neuron is described by the adaptive exponential integrate-and-fire model (AEIF) [15]

$$C_{\mathrm{m}}\frac{dV_i}{dt} = -g_{\mathrm{L}}(V_i - E_{\mathrm{L}}) + g_{\mathrm{L}}\Delta_{\mathrm{T}}\exp\left(\frac{V_i - V_{\mathrm{T}}}{\Delta_{\mathrm{T}}}\right) - w_i + I_i, + \sum_{k=1}^{N}(V_{\mathrm{REV}}^{k} - V_i)g_k M_{ik}, \tag{30.1}$$

$$\tau_w\frac{dw_i}{dt} = a(V_i - E_{\mathrm{L}}) - w_i, \tag{30.2}$$

$$\tau_{\mathrm{g}}\frac{dg_i}{dt} = -g_i, \tag{30.3}$$

where V_i, w_i and g_i are the membrane potential, adaptive current and synaptic conductance of neuron i, respectively. C_{m} is the membrane capacitance, g_{L} is the leak conductance, E_{L} is the resting potential, Δ_{T} is the slope factor, V_{T} is the threshold potential, I_i is the applied constant current, V_{REV}^{k} is the reversal potential of neuron k ($V_{\mathrm{REV}}^{\mathrm{exc}} = 0$ mV and $V_{\mathrm{REV}}^{\mathrm{inh}} = -80$ mV), M_{ik} is the adjacency matrix, τ_w is the adaptive current time constant, a is the, τ_{g} is the synaptic time constant. Reset conditions in V_i, w_i and g_i are applied when the neuron membrane potential surpasses a maximum value ($V_i \geq V_{\max}$); $V_i \to V_{\mathrm{reset}}$, $w_i \to w_i + b$ and $g_i \to g_i + g_{\mathrm{syn}}$. Where V_{reset} is the reset potential, b is an increase in the adaptive current and g_{syn} is an increment in the synapse conductance. In our simulations, we consider $C_{\mathrm{m}} = 200$ pF, $g_{\mathrm{L}} = 12$ nS, $E_{\mathrm{L}} = -70$ mV, $\Delta_{\mathrm{T}} = 2$ mV, $V_{\mathrm{T}} = -50$ mV, $I_i = 512$ pA, $\tau_w = 300$ ms, $a = 2$ nS, $\tau_{\mathrm{g}} = 1.5$ ms $V_{\mathrm{reset}} = -58$ mV and $b = 70$ pA. V and w initial condition are randomly chosen in the range [–75, –45] mV and [0, 70] pA, respectively, $g_i(0) = 0$ nS.

Despite the model's simplicity, it reproduces many firing patterns with different combinations of (V_{reset}, b) [20, 21]. Figure 30.1a–e shows five firing patterns that the model reproduces for a single neuron ($g_i \to 0$). The panel (a) displays adaptive spiking, initially, the firing frequency is high, however, it decreases over time until it reaches a constant value lower than in the beginning. Tonic spiking, unlike adaptive spiking, has a constant firing rate, the panel (b). Some combinations of reset parameters produce initial bursting, as depicted in the panel (c). The panels (d) and (e) display regular and irregular bursting, respectively. The interburst interval is constant in regular bursting, which does not hold for irregular bursting [20]. Figure 30.1f shows the applied current influence over the frequency rate of a single neuron. Each

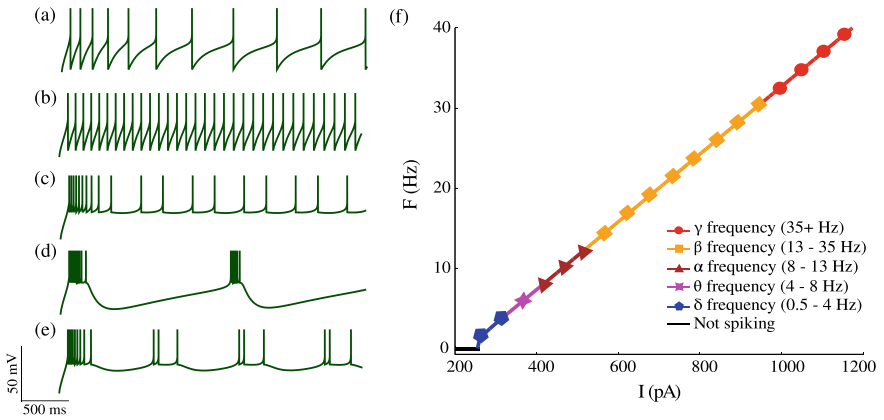


Fig. 30.1 Panels (**a**–**e**) show the firing patterns which the AEIF model produces with different combinations of V_{reset} and b, in these panels we consider $I = 512$ pA. **a** adaptive spiking ($V_{\text{reset}} = -68$ mV, $b = 60$ pA), **b** tonic spiking ($V_{\text{reset}} = -65$ mV, $b = 5$ pA), **c** initial bursting ($V_{\text{reset}} = -48.8$ mV, $b = 35$ pA), **d** regular spiking ($V_{\text{reset}} = -45$ mV, $b = 40$ pA) and **e** irregular spiking ($V_{\text{reset}} = -47.4$ mV, $b = 41$ pA). Panel **f** exhibits the frequency response of one neuron for different values of applied current (I)

symbol and color represent a specific frequency band black line for no spike is generated, blue hexagons for δ, magenta star for θ, brown triangle for α, yellow square for β, red circles for γ frequency band. The linear relation of F and I is given by $F = 0.04I - 9.39$. For $I < 260$ pA, spikes are not generated, due to the fact that it is below the rheobase current value [15, 20].

We constructed a simplified hippocampus pyramidal layer composed of excitatory neurons, we consider one 1000×1000 μm 2D layer. The distance of two neurons is 7 μm in the x-axis and 8 μm in the y-axis [13]. To maintain the experimental neuronal superficial density [13], we consider 17,324 neurons. The neuron i is connected with its neighbors that are within the radius r ($M_{ij} = 1$), where r origin is the center of neuron i. No connections exist with neurons outside the radius r ($M_{ij} = 0$).

Statistical tools can be used to identify the type of firing pattern, such as the coefficient of variation CV of the neuronal inter-spike interval (ISI) [18, 20]. ISI is defined as $\text{ISI}_i = t_i^{m+1} - t_i^m$ where t_i^m is m-th spike time of the neuron i. CV is given by $\text{CV} = \frac{\sigma_{\text{ISI}}}{\overline{\text{ISI}}}$, where σ_{ISI} is the standard deviation of ISI and $\overline{\text{ISI}}$ is the network mean value of ISI [22]. For the AEIF model, CV$<$0.5 is produced when the network firing pattern is spike and CV$\geq$0.5 represents bursting activity. The mean frequency F of the network is defined as $\text{F} = \overline{\text{ISI}}^{-1}$.

One quantitative measure of synchronization is the Kuramoto order parameter (Z(t)) [23, 24]. We consider, the global Kuramoto order parameter Eq. 30.4

$$\text{R}(t) = \left| \frac{1}{N} \sum_{j=1}^{N} \exp\left(i\phi_j(t)\right) \right|, \tag{30.4}$$

ϕ_j is the j-neuron phase defined by Eq. 30.5

$$\phi_j(t) = 2\pi m + 2\pi \frac{t - t_j^m}{t_j^{m+1} - t_j}, \tag{30.5}$$

where m is the m-th firing of the j-neuron ($m = 1, 2, 3, \dots$) and t_j^m is the time of the m-th spiking. Total synchronization and desynchronization are characterized by $\mathrm{R}(t) = 1$ and $\mathrm{R}(t) = 0$, respectively, when $0 < \mathrm{R}(t) < 1$ partial synchronization is observed [25]. To study the network activity, we calculate the mean value of $\mathrm{R}(t)$ along the time interval $t_{\text{initial}} = 15$ s and $t_{\text{final}} = 20$s to avoid transient effects.

$$\mathrm{R_g} = \frac{1}{t_{\text{final}} - t_{\text{initial}}} \int_{t_{\text{initial}}}^{t_{\text{final}}} \mathrm{R}(t)dt. \tag{30.6}$$

To identify global synchronization, we set the threshold $\mathrm{R}_g < 0.7$ the network is desynchronized and $\mathrm{R}_g \geq 0.7$ the network is synchronized. To evaluate local synchronization of each neuron we separated the 1000×1000 μm layer into 625 boxes, with dimensions 40×40 μm, each box contains 28 neurons. The boxes are labeled by the subindex (l, m) where l represents the l-th box in x-axis ($l = [1, 25]$) and m is the m-th box in y-axis ($m = [1, 25]$). The local Kuramoto order parameter of (l, m)-box is given by the sum of Euler's exponential of the phase of the j-neurons inside the (l, m)-box

$$\mathrm{R}_{l,m}(t) = \left| \frac{A^2}{N^2} \sum_{\substack{n=j \\ \in(l,m)}} \exp(i\phi_n) \right|, \tag{30.7}$$

where A is the number of boxes and j is the index of a neuron ($j = [1, 17324]$). The temporal mean of $\mathrm{R}_{l,m}$ is

$$\overline{\mathrm{R}}_{l,m} = \frac{1}{t_{\text{final}} - t_{\text{initial}}} \int_{t_{\text{initial}}}^{t_{\text{final}}} \mathrm{R}_{l,m}(t)dt, \tag{30.8}$$

and the network average local Kuramoto order parameter is

$$\mathrm{R_L} = \frac{1}{A} \sum_{l,m}^{25} \overline{\mathrm{R}}_{l,m}, \tag{30.9}$$

where $A = 625$ is the number of boxes.

30.3 Results

There are different brain wave patterns such as plane, ring, spiral and others. Figure 30.2 shows six wave patterns throughout the time that our network generates for different (r, g_{syn}) combinations. The panel (a) displays the ring wave pattern, global synchronization produces this wave pattern. The panel (b) exhibits multi-ring waves. The rings appear and propagate at different time instants. The difference between the ring and multi-ring waves is the global synchronization, the multi-ring is only locally synchronized. Spiral waves are seen in a variety of systems such as heart tissue models [26], complex oscillators [27] and chemical oscillators [28]. The center of spiral waves are called phase singularities which are composed of asynchronous elements. The panel (c) displays a single spiral wave rotating around its phase singularity. More than one spiral can exist simultaneously, the panel (d) shows the presence of two spiral waves with distinct phase singularities. Each spiral rotates in a different direction. Bursting spiral wave is displayed in the panel (e). This pattern is observed for r $>$ 60 μm and it behaves as the spike spiral wave. The panel (f) exhibits the coexistence of two different wave patterns multi-ring and multi-spiral waves, we denote this pattern as multi-spiral-rings.

In Fig. 30.3, we analyze the global and local synchronization and the frequency for the cases in Fig. 30.2. The synchronization measurements of each wave pattern

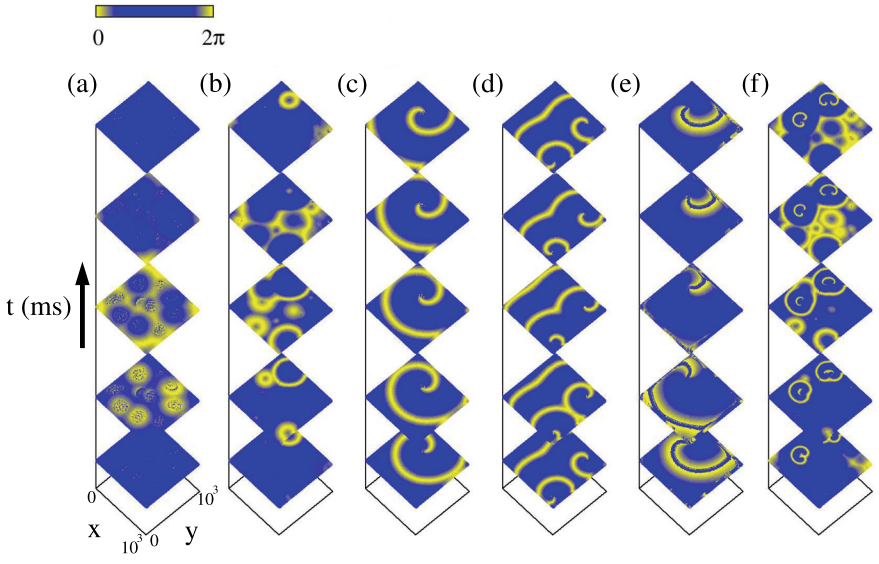


Fig. 30.2 Wave patterns for different combinations of r and g_{syn}. **a** synchronized ring wave r = 55 μm and g_{syn} = 0.16 nS, **b** multi-ring wave r = 32 μm and g_{syn} = 0.15 nS, **c** spiral wave r = 70 μm and g_{syn} = 0.12 nS, **d** multi-spiral wave r = 50 μm and g_{syn} = 0.24 nS, **e** burting spiral wave r = 75 μm and g_{syn} = 0.14 nS and **f** multi-spiral-rings r = 30 μm and g_{syn} = 0.15 nS. R_g, R_L and F of each wave pattern is shown in Fig. 30.3

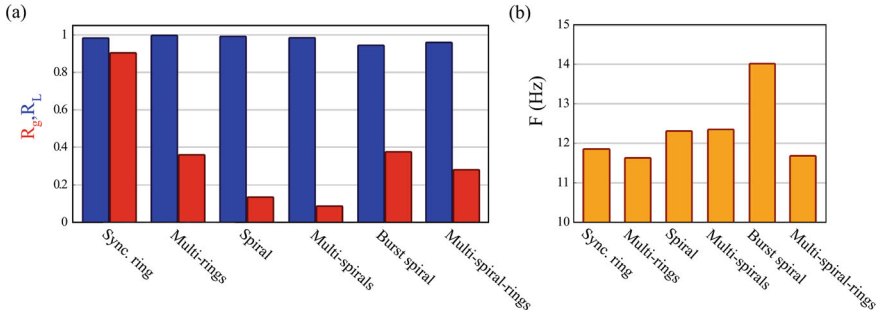


Fig. 30.3 Diagnostic tools for the wave patterns studied. **a** R_g in red and R_L in blue and **b** frequency F and CV

are exhibited in the panel (a). The synchronized ring pattern produces local and global synchronization, $R_g > 0.8$ and $R_L \approx 1$. Synchronization generates this wave pattern, each ring starts expanding at the same time. Despite the distinct spatial pattern of each wave, they possess a similar characteristic which is local synchronization and global desynchronization. If $R_g < 0.7$ and $R_L \approx 1$, waves are observed in the network. Multi-spiral waves generate a lower global synchronization than a single spiral, this is also observed between multi-rings and multi-spiral-ring patterns. The panel (b) shows the F and the CV for the cases studied. The frequency of all cases does not change significantly, they stay in the range of the β frequency (13–35 Hz). $CV > 0.5$ only in the bursting spiral, this yields that for the other cases the neurons are in regular spike.

Lastly, we study $\overline{R}_{l,m}$ of the wave patterns considered. Figure 30.4 displays $\overline{R}_{l,m}$ for synchronous ring (panel (a)), multi-ring (panel (b)), spiral (panel (c)), multi-spiral (panel (d)), bursting spiral (panel (e)) and multi-spiral-rings (panel (f)). In the panel (a), the center of the rings has $\overline{R}_{l,m} \approx 0.85$. In the panels (c-f), there are desynchronized regions (dark colors $\overline{R}_{l,m} < 0.7$). Spiral waves create in their center a phase singularity (PS) which is composed of asynchronous elements. We observe that PS is detected by low values of $\overline{R}_{l,m}$, $\overline{R}_{l,m} < 0.7$. One PS is seen on the panel (c) due to the presence of a single spiral. Two distinct spirals generate their own phase singularity in their core on the panel (d). The panel (e) exhibits $\overline{R}_{l,m}$ for the bursting spiral wave, this pattern generates border effects. $\overline{R}_{l,m} < 0.7$ in the border cannot be considered as PS because no spiral wave is orbiting them. The panel (f) shows four PS in the multi-spiral-rings, the far regions from the PSs are similar to the multi-rings case (panel (b)).

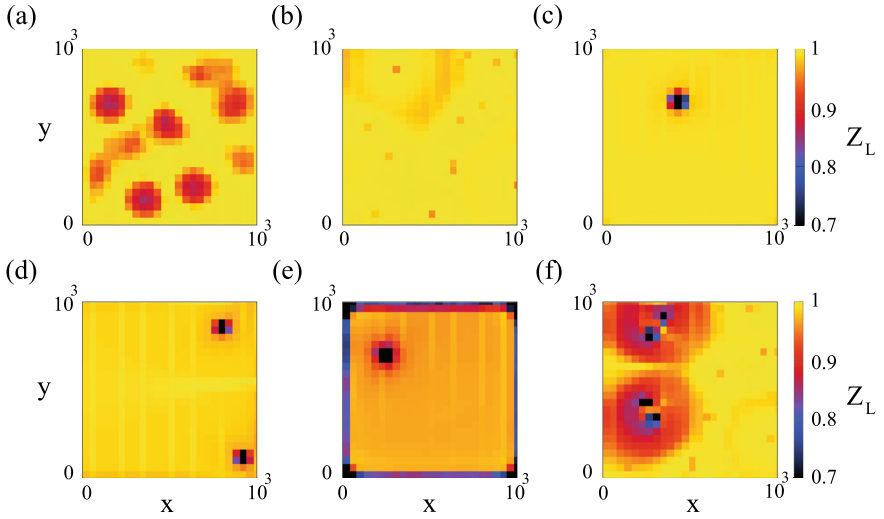


Fig. 30.4 Mean local order parameter of each neuron $\overline{R}_{l,m}$ for all cases studied. **a** synchronized rings, **b** multi-rings, **c** spiral, **d** multi-spiral, **e** bursting spiral and **f** multi-spiral-rings

30.4 Conclusions

The organized firing of neurons produces traveling waves in the brain. In the hippocampus, this oscillatory behavior is associated with episodic memory and spatial localization. Therefore understanding the trigger of the emergence of waves and their influence over the network is essential. We construct a hippocampal network composed of pyramidal neurons described by the adaptive exponential integrate-and-fire model. In our network, each neuron connects to its neighbors within a connection radius (r) with an excitatory coupling strength (g_{syn}).

In this work, we show that some combinations of connection radius and coupling strength generate different wave patterns in a 2D hippocampus network. The patterns that we observed are synchronized rings, multi-rings, spiral, multi-spiral, bursting spiral and multi-spiral-rings waves. R_L is high for all wave patterns since only neurons that are near fire when a wave passes. We show this phenomenon for all cases studied here, except in the bursting spiral that some neurons in the border fire at random times due to border effects. Synchronized rings are the only pattern that produces $R_g > 0.9$ because all rings start at the same time and propagate at the same rate. The other wave patterns are not globally synchronized because only local neurons fire together when the wave passes. R_g of the multi-spiral is lower than the case where only one spiral is observed, this same behavior is seen comparing R_g of multi-ring and multi-spiral-ring. We theorized that the presence of phase singularities directly affects global synchronizations. Therefore, as more simultaneous spiral waves appear the network tends to desynchronize.

The mean local order parameter ($\overline{R}_{i,j}$) of synchronized and multi rings do not show information about the wave patterns. Although, spiral waves are characterized with $\overline{R}_{i,j}$ by detecting the phase singularity. In the core of the spirals of each case studied the phase singularities produce $\overline{R}_{i,j} < 0.7$. Figure 30.4e has more regions of $\overline{R}_{i,j} < 0.7$ due to border effects. Locating the center of the spiral allows us to know when a spiral wave is in our system, however, we do not have any information about wave direction and velocity. In conclusion, this study highlights how a simplified neuronal model faithfully reproduces complex oscillations present in the mammalian brain, elucidating the synchronization properties of wave patterns.

Acknowledgements This work was possible by partial financial support from the following Brazilian government agencies: CNPq, CAPES, and São Paulo Research Foundation (FAPESP 2018/03211-6). We would like to thank http://www.105groupscience.com.

Declarations

Conflict of Interest The author declares that there exists no competing financial interest or personal relationships that could have appeared to influence the work reported in this paper.

Funding D.L.M.S received financial support from Coordenação de Aperfeiçoamento de Pessoal de Nível Superior—Brazil (CAPES)—Finance Code 88887.849164/2023-00. L.E.B received financial support from Coordenação de Aperfeiçoamento de Pessoal de Nível Superior—Brazil (CAPES)—Finance Code 88887.702524/2022-00. P.D.C.R. received financial support from Coordenação de Aperfeiçoamento de Pessoal de Nível Superior—Brazil (CAPES)—Finance Code 88887.856951/2023-00. I.L.C. received financial support from Fundação de Amparo à Pesquisa do Estado de São Paulo, processo FAPESP 2018/03211-6. R.L. V. received partial financial support from the following Brazilian government agencies: CNPq (403120/2021-7, 301019/2019-3), CAPES (88881.143103/2017-01), FAPESP (2022/04251-7).

Author Contribution All authors discussed the results and contributed to the final manuscript.

References

1. Omelchenko, I., Omel'chenko, O.E., Hövel, P., Schöll, E.: When nonlocal coupling between oscillators becomes stronger: patched synchrony or multichimera states. Phys. Rev. Lett. **110**, 224101 (2013)
2. Aristides, R.P., Viana, R.L.: Non-local coupling among oscillators mediated by fast traveling waves. Int. J. Nonlinear Dyn. Control. 376–386 (2019)
3. Stoelzel, C.R., Bereshpolova, Y., Alonso, J., Swadlow, H.A.: Axonal conduction delays, brain state, and corticogeniculate communication. J. Neurosci. 6342–6358 (2017)
4. Muller, L., Chavane, F., Reynolds, J., Sejnowski, T.J.: Cortical traveling waves: mechanisms and computational principles. Nat. Rev. Neurosci. (2018)
5. Uzelac, I., Iravanian, S., Bhatia, N., Fenton, F.H.: Spiral wave breakup: optical mapping in an explanted human heart shows the 379 transition from ventricular tachycardia to ventricular fibrillation and self-termination. Hear. Rhythm. **19**, 1914–1915 (2022)
6. Huang, X., Xu, W., Liang, J., Takagaki, K., Gao, X., Wul, J.: Spiral wave dynamics in neocortex. Neuron **68**, 978–990 (2010)

7. Patten, T.M., Rennie, C.J., Robinson, P.A., Gong, P.: Human cortical traveling waves: dynamical properties and correlations with responses. PLoS ONE **7**(6), e38392 (2012)
8. Buzsaki, G.: Rhythms of the Brain. OUP, New York (2006)
9. Zhang, H., Jacob, J.: Traveling theta waves in the human hippocampus. J. Neurosci. **35**(36), 12477–12487 (2015)
10. Molter, C., Sato, N., Yamagucho, Y.: Reactivation of behavioral activity during sharp waves: a computational model for two stage hippocampal dynamics. Hippocampus **17**, 201–209 (2007)
11. Yao, Y., Deng, H., Yi, M., Ma, J.: Impact of bounded noise on the formation and instability of spiral wave in a 2D Lattice of neurons. Sci. Rep. **7**, 43151 (2017)
12. Wang, Q., Perc, M., Duan, Z., Chen, G.: Delay-enhanced coherence of spiral waves in noisy Hodgkin-Huxley neuronal networks. Phys. Lett. A **372**, 5681–5687 (2008)
13. Bezaire, M.J., Raikov, I., Burk, K., Vyas, D., Soltesz, I.: Interneuronal mechanisms of hippocampal theta oscillations in a full-scale model of the rodent CA1 circuit. eLife 5e18566 (2016)
14. Bekkers, J.M.: Pyramidal neurons. Current Biology, Quick Guide **21**(24), PR975 (2011)
15. Brette, R., Gerstner, W.: Adaptive exponential integrate-and-fire model as an effective description of neuronal activity. J. Neurophysiol. **94**, 3637–3642 (2005)
16. Protachevicz, P.R., Hansen, M., Iarosz, K.C., Caldas, I.L., Batista, A.M., Kurths, J.: Emergence of neuronal synchronisation in coupled areas. Front. Comput. Neusocience **15**, (2021)
17. Protachevicz, P.R., Borges, F.S., Lameu, E.L., Ji, P., Iarosz, K.C., Kihara, A.H., Caldas, I.L., Szezech, J.D., Jr., Baptista, M.S., Macau, E.E.N., Antonopoulos, C.G., Batista, A.M., Kurths, J.: Bistable firing pattern in a neural network model. Front. Comput. Neurosci. **13**, 1–8 (2019)
18. Borges, F.S., Gabrick, E.C., Protachevicz, P.R., Higa, G.S.V., Lameu, E.L., Rodriguez, P.X.R., Ferraz, M.S.A., Szezech, J.D.J., Batista, A.M., Kihara, A.H.: Intermittency properties in a temporal lobe epilepsy model. Epilepsy & Behav. **139**, 109072 (2023)
19. Zhang, Q., Zeng, Y., Zhang, T., Yang, T.: Comparison between human and rodent neurons for persistent activity performance. A biologically plausible computational investigation. Front. Syst. Neurosci. 15 (2015)
20. Naud, R., Marcille, N., Clopath, C., Gerstner, W.: Firing patterns in the adaptive exponential integrate-and-fire model. Biol. Cybern. **99**, 335–347 (2008)
21. Souza, D.L.M., Gabrick, E.C., Protachevicz, P.R., Borges, F.S., Trobia, J., Iarosz, K.C., Batista, A.M., Caldas, I.L., Lenzi, E.K.: Adaptive exponential integrate-and-fire model with fractal extension. Chaos **34**, 023107 (2024)
22. Gabbiani, F., Koch, C.: Principles of Spike Train Analysis, in Methods in Neuronal Modeling: From Ions to Networks. In: Koch, C., Segev, I (eds.), 2nd edn, pp. 313–360. Cambridge, MA, MIT Press (1998)
23. Borges, F.S., Protachevicz, P.R., Souza, D.L.M., Bittencourt, C.F., Gabrick, E.C., Bentivoglio, L.E., Szezech, J.D., Jr., Batista, A.M., Caldas, I.L., Dura-Bernal, S., Pena, R.F.O.: The roles of potassium and calcium currents in the bistable firing transition. Brain Sci. **13**, 1347 (2023)
24. Ferrari, F.A.S., Viana, R.L., Lopes, S.R., Stoop, R.: Phase synchronization of coupled bursting neurons and the generalized Kuramoto model. Neural Netw. (2015), 107–118
25. Kuramoto, Y.: Chemical Oscillations, Waves, and Turbulence. Springer-Verlag, Berlin (1984)
26. Ding, Q., Wu, Y., Hu, Y., Liu, C., Hu, X., Jia, Y.: Tracing the elimination of reentry spiral waves in defibrillation: temperature effects. Chaos Solitons Fractals (2023), 113760
27. Gu, C., St-Yves, G., Davidsen, J.: Spiral wave chimeras in complex oscillatory and chaotic systems. Phys. Rev. Lett. **111**, 134101 (2013)
28. Totz, J.F., Rode, J., Tinsley, M.R., Showalter, K., Engel, H.: Spiral wave chimera states in large populations of coupled chemical oscillators. Nat. Phys. **14**, 282–285 (2018)